Research Square

Preprints are preliminary reports that have not undergone peer review.
They should not be considered conclusive, used to inform clinical practice,
or referenced by the media as validated information.

Electrochemical Impedance Analysis on Hydrated 3YSZ and 8YSZ Nanopowders

Anthony C. Perez M.

anthonycpm@jinr.ru

Joint Institute for Nuclear Research

Mahmoud A. Ibrahim

Joint Institute for Nuclear Research

Zhanna V. Mezentseva

Joint Institute for Nuclear Research

Dmitry E. Lyubashevsky

Voronezh State University

Evgeniy V. Lukin

Joint Institute for Nuclear Research

Aleksandr S. Doroshkevich

Joint Institute for Nuclear Research

Research Article

Keywords: Equivalent circuit, Humidity sensor, Impedance spectroscopy, Nanoparticles, Proton conduction, YSZ.

Posted Date: November 17th, 2026

DOI: https://doi.org/10.21203/rs.3.rs-11625404/v1

License: This work is licensed under a Creative Commons Attribution 4.0 International License.
Read Full License

Additional Declarations: No competing interests reported.

Electrochemical Impedance Analysis on Hydrated 3YSZ and 8YSZ Nanopowders

Anthony C. Perez M.[1,2]*, Mahmoud A. Ibrahim[1,3], Zhanna V. Mezentseva[1], Dmitry E. Lyubashevsky[2], Evgeniy V. Lukin[1], Aleksandr S. Doroshkevich[1,4]

anthonycpm@jinr.ru

[1]Joint Institute for Nuclear Research, 141980, Dubna, Joliot Curie St. No. 6, Russian Federation

[2]Voronezh State University, 394018, Voronezh, Universitetskaya pl., No. 1, Russian Federation

[3] Division for Experimental Physics, National Research Tomsk Polytechnic University, Tomsk, 634050, Russian Federation

[4] Ural Federal University named after the first President of Russia B.N.Yeltsin, Ekaterinburg, , 19 Mira Street, 620002, Russian Federation

Abstract

The effect of humidity on the electrical impedance of zirconia nanoparticles stabilized with two different yttria contents (3 mol% and 8 mol% Y_2O_3), both with a size distribution ranging from 7 to 10 nm, as confirmed by TEM (Transmission Electron Microscopy) , was examined. Impedance measurements were performed after four different exposure times (4, 32, 54, and 70 minutes), maintaining a constant relative humidity of 100%. A combined model was developed that links the charge carrier transport mechanisms (proton conduction via Grotthuss and vehicular mechanisms) with an equivalent circuit representation of the impedance response. To monitor the evolution of the impedance response, an equivalent circuit was developed, incorporating bulk (high-frequency), grain boundary (intermediate-frequency), and diffusion (low-frequency) contributions. The results are consistent with the formation of a proton conduction pathway via these mechanisms in the physisorbed water layers for both 3YSZ and 8YSZ compositions. These results contribute to the understanding of humidity-induced proton conduction in YSZ nanopowders, establishing the basis for their application as humidity-activated gas sensors at room temperature (26 to 30 °C).

Keywords:

Equivalent circuit, Humidity sensor, Impedance spectroscopy, Nanoparticles, Proton conduction, YSZ.

1. Introduction

Oxide systems in the form of nanoparticles are promising for gas analysis [1,2]. In particular, YSZ nanostructures have attracted interest for applications such as gas sensors and low-temperature electrochemical devices, where the surface-to-volume ratio of nanoparticles plays a decisive role [3,4].

YSZ nanoparticles have the characteristic that under humid conditions, their surface becomes covered with adsorbed water molecules, which dissociate into hydroxyl groups (OH^-) and protons (H^+) [5,6]. These hydroxyl ions interact with surface oxygen vacancies, modifying the chemistry of local defects and inducing structural changes in the near-surface region [7]. In this context, the product of dissociative water adsorption on the surface of YSZ nanoparticles can act as an electrolyte, forming an ionic atmosphere that contributes to the formation of a double electric layer at the heterophase boundary [2].

It is common practice to use electrochemical impedance spectroscopy as a technique to investigate electrical transport in ionic and mixed conductors, since it allows us to separate the resistances of the bulk and the grain boundary, as well as electrode contributions by modeling equivalent circuits [1,8,9]. In the specific case of electrochemical sensors employing nanomaterials, the use of this technique is particularly widespread, given that these materials offer significant advantages, such as a larger effective sensor surface area, improved electrical conductivity and connectivity, greater chemical accessibility, and enhanced electrocatalytic activity [10,11].

YSZ-based systems typically exhibit one or two semicircles in the complex plane, depending on the microstructural complexity and the presence of surface or interfacial phenomena [12,13]. However, interpreting impedance data in terms of equivalent circuits remains challenging when multiple processes overlap, such as operation in high relative humidity environments.

In this work, we investigated the electrical properties of YSZ nanoparticles with two different yttria contents (3 mol% and 8 mol% Y_2O_3) under 100% relative humidity using electrochemical impedance spectroscopy.

The objectives of this work are: (i) to analyze the charge carrier transport model, (ii) to develop an equivalent circuit that accurately models the impedance response of our system, (iii) to identify the behavior of the sensors over time when exposed to an environment of 100% relative humidity, (iv) to compare the effect of yttria concentration on the observed phenomena, and (v) to establish a foundation for the application of hydrated YSZ nanopowders as humidity-activated gas sensors operating at room temperature (26 to 30 °C).

2. Materials and Methods

Crystalline yttria-stabilized zirconia (YSZ) nanopowders with compositions of 8 mol% Y_2O_3 (8YSZ) and 3 mol% Y_2O_3 (3YSZ) were synthesized by a coprecipitation method using zirconium chloride ($ZrOCl_2$) and yttrium chloride (YCl_3) as precursors. These samples were calcined at 400 °C, resulting in particles with size distribution ranging from 7 to 10 nm.

For impedance analysis, a solution of these compounds was mixed with a polyvinyl acetate (PVAc) matrix. The sensing layer was deposited using the drop-casting method onto a substrate with two gold-plated copper electrodes (Figure

1a). Finally, the device (sensor) was allowed to dry at room temperature to evaporate the solvent and form the active film.

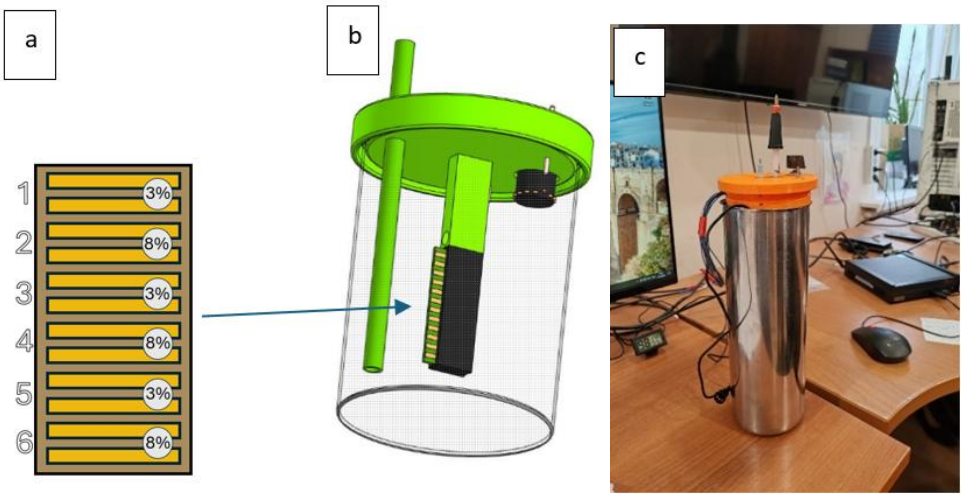


Figure 1. Representation of sensors based on yttria-stabilized zirconia (YSZ), 3 mol% Y_2O_3 (3YSZ) and 8 mol% Y_2O_3 (8YSZ) on gold-plated copper electrodes (a), schema of the humidity-controlled chamber for the experiment (b) and the external view of the chamber.

The experiments were conducted in a chamber with 100% relative humidity (Figure 1b, c), using distilled water. This humidity was maintained throughout the experiment.

To investigate the electrical response of YSZ samples, they were deposited in a container with 100% relative humidity. The analysis began 4 minutes after deposition inside the humid chamber, and four measurements were performed for each sensor. The temperature inside the container remained around 26 to 30 °C throughout the experiment.

The impedance was measured with a P-45X potentiostat-galvanostat device. The measurement frequencies ranged from 1 MHz to 1 Hz, and the nominal AC voltage used was 100 mV.

The Aftermath software release 1.6.10523 (Pine Research Instrumentation, Durham, NC, USA) [14] was used to process the spectra obtained from the experiments.

3. Results

3.1. Transmission Electron Microscopy (TEM) analysis of Yttria Stabilized Zirconia (3YSZ and 8YSZ)

The nanoscale morphology of the 3YSZ and 8YSZ nanopowders was analyzed by transmission electron microscopy (TEM) using a JEOL, JEM 200A (Tokyo, Japan). The representative TEM micrographs are shown in Figure 2.

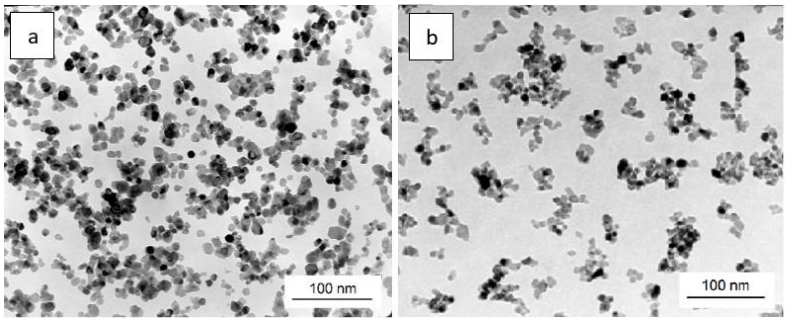


Figure 2. The TEM images of the nanopowders with the composition 3YSZ (a) and 8YSZ (b), (400 °C for 2 h).

The TEM results reveal that both nanopowders consist predominantly of spherical nanoparticles with a primary particle size distribution of approximately 7 to 10 nm. The nanopowders are distributed almost uniformly, forming aggregates with sizes between 20 and 70 nm.

The morphology of 3YSZ and 8YSZ is essentially identical, showing that the yttria content does not significantly influence the particle size or aggregation state. The presence of agglomerates is relevant for the impedance analysis, as they create a dense network of grain boundaries that can facilitate the formation of proton conduction pathways [15,16].

3.2. X-Ray Diffraction (XRD) Analysis of YSZ Nanopowders of Yttria Stabilized Zirconia (3YSZ and 8YSZ)

The crystalline structure of the nanopowders was analyzed by X-ray diffraction (XRD) using a PANalytical diffractometer with filtered Cu-Kα radiation (λ = 1.541889 Å). The resulting patterns, recorded in the 2θ range of 20–55°, are presented in Figure 3.

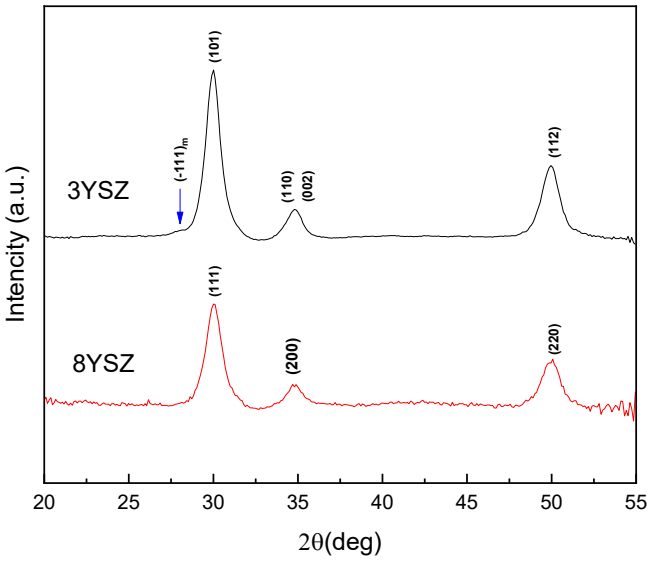


Figure 3. XRD patterns of nanopowders 3YSZ and 8YSZ calcined at 400 °C

For the sample 8YSZ, the pattern exhibits the characteristic reflections of the cubic fluorite structure (JCPDS No. 30-1468). The most intense peak at 2θ ≈ 30.0° corresponds to the (111) reflection, followed by the (200) and (220) reflections at

approximately 35.0° and 50.0°, respectively. The presence of a single, well-defined (200) peak confirms the cubic symmetry, as no splitting is observed in this region [17].

In the case of the 3YSZ sample, the characteristic pattern of the tetragonal phase (JCPDS No. 48-0224), can be observed. The most intense reflection at 2θ ≈ 30.2° corresponds to the (101) plane. The tetragonal structure is evidenced by the splitting of the (110) and (002) reflections at approximately 2θ ≈ 34.8° and 35.2°, respectively, followed by the (112) peaks at higher angles (2θ ≈ 50.2°). Additionally, a small, broad reflection is detected at approximately 2θ ≈ 28°, with a peak at $(-111)_m$ which can be attributed to a minor fraction of the monoclinic phase. This is a common feature in zirconia with low yttria content (3 mol%) [17], however no monoclinic peaks are observed in the 8YSZ pattern, confirming the fully stabilized cubic phase. The average crystallite size (D) was estimated using the Scherrer equation:

$$D = (0.9\lambda) / (\beta \cos\theta)$$

where λ is the X-ray wavelength, β is the full width at half maximum (FWHM) of the most intense peak, and θ is the Bragg angle. The 2θ positions were calibrated using a LaB_6 standard, and the instrumental broadening was determined from the LaB_6 FWHM at the corresponding 2θ values. Using the (101) reflection for 3YSZ and the (111) reflection for 8YSZ, the calculated crystallite sizes are approximately 9.06 nm and 8.54 nm, respectively, which are consistent with the particle size distribution observed by TEM (7–10 nm). The slight difference between the two compositions may be attributed to the higher yttria content in 8YSZ, which can influence the nucleation and growth kinetics during calcination [18].

3.3. Electrochemical Impedance Spectroscopy (EIS)

Figure 4 shows the complex impedance plots (Nyquist diagrams) for the four measurements (1E, 2E, 3E, and 4E) of the 3YSZ (a, b) and 8YSZ (c, d) sensors during water adsorption at 100% RH. Panels (a) and (c) present the complex impedance response for the four measurements. Panels (b) and (d) show an enlarged view of measurements 2E (32 min), 3E (54 min), and 4E (1 h 10 min), which are contained within panels (a) and (c).

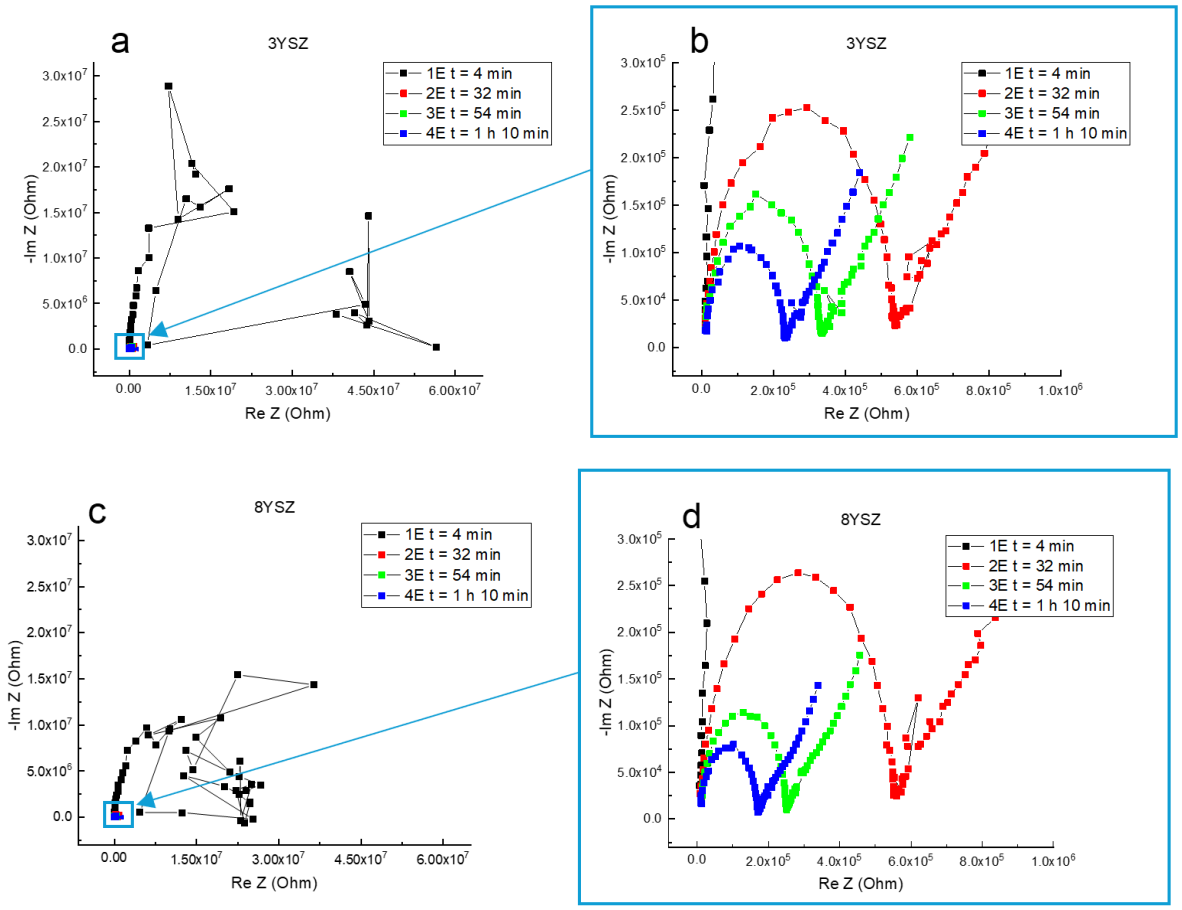


Figure 4. Complex impedance plots for the 3YSZ (a, b) and 8YSZ (c, d) sensors during water adsorption at 100% RH.

In both samples, the onset of semicircles located in the high-frequency region (Re Z < 1×10⁵ Ω) can be observed; these remain virtually unchanged with exposure time. The first semicircle, located in the intermediate-frequency region (6×10⁵ Ω > Re Z > 1×10⁵ Ω), is clearly visible and shows a marked decrease as exposure time increases. Notably, at 4 min (1E), the semicircle is so large (Re Z > 5×10⁷ Ω for 3YSZ and > 2.5×10⁷ Ω for 8YSZ) that it does not close within the measured frequency range, indicating high initial resistance. As can be seen, the semicircles progressively contract (2E, 3E, 4E) as the sensors remain exposed to high-humidity conditions. This reduction is attributable to the formation of a proton-conduction pathway along hydrated grain boundaries, as discussed in Section 4.1.1.

In measurements 2E, 3E, and 4E, a second arc appears at lower frequencies, corresponding to the diffusion of reactive species through the hydrated surface layer. In measurement 1E, this arc is not visible because it is masked by the large size of the first semicircle.

4. Results

4.1. Charge carrier transport model

4.1.1. Surface Conductivity of Hydrated YSZ Nanoparticles

It can be observed that under dry or low-humidity conditions, the samples exhibit capacitive behavior related to the material's dielectric constant [19].

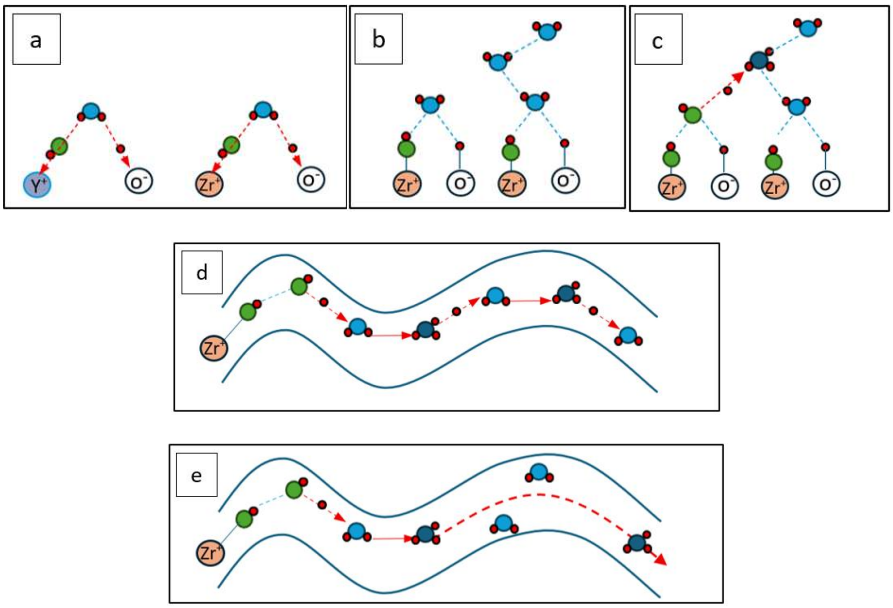
Similarly, a significant change in impedance response is observed as exposure time to high humidity increases, manifesting as a notable drop in the real component of impedance. This phenomenon can be attributed primarily to two complementary mechanisms:

a. Humidity-induced proton conduction

Under conditions of high relative humidity, water molecules dissociate into H^+ and OH^-. The hydroxyl groups (OH^-) bind to surface metal ions (Zr^{4+} and Y^{3+}), while the protons (H^+) associate with surface oxygen sites (O^{2-}), generating additional hydroxyl groups (OH^-) that bind to surface oxygen vacancies (chemisorption, Figure 5a). This chemisorption process forms a fairly stable first layer. Once the first layer is formed, a second layer, known as the physisorption layer, is generated. This layer is composed of undecomposed water molecules held together by double hydrogen bonds. Subsequent physisorption layers, unlike the first layer, are held together by single hydrogen bonds, the same behavior as liquid water (Figure 5b) [20]. It is in these physisorbed layers where proton transfer occurs, with conduction in these layers being dominant (Figure 5c) [21]. Two primary proton transport mechanisms have been identified [22,23]:

- **Grotthuss mechanism (structural diffusion):** This mechanism is present in the initial physisorption layers, where protons are transported via successive hops along a hydrogen-bonded network of water molecules (Figure 5d), without the physical displacement of individual water molecules. The proton effectively moves as a "charge defect" through the water network, rapidly jumping between adjacent molecules.
- **Vehicular mechanism:** In this mechanism, the proton is transported together with a water molecule, forming a hydronium ion (H_3O^+), which diffuses through the water layer (Figure 5e). This mechanism becomes dominant in the outer physisorbed water layers, which adopt a more liquid-like structure, similar to bulk water.

These protons are then transported to adjacent molecules via these mechanisms, resulting in an ionic conduction pathway (Figure 5f), which is practically absent under low humidity conditions [22, 24].



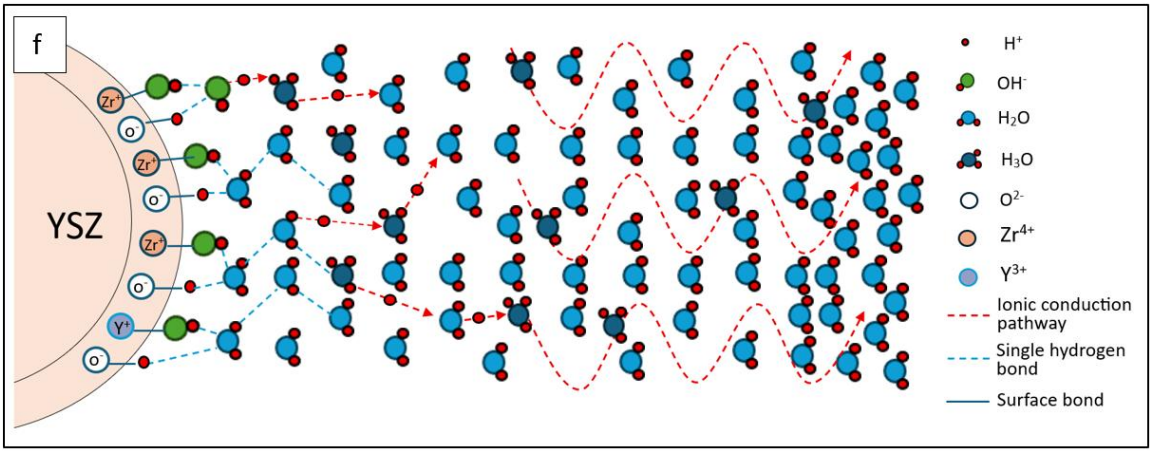


Figure 5. Mechanism for adsorption of water molecules on the surface of zirconia (a) chemisorption process, (b) physisorption of water, (c) proton transport in the physisorption layer, (d) Grotthuss mechanism for proton transport, (e) Vehicular mechanism of proton transport, (f) ion conduction mechanism.

b. High density of surface-active sites and grain boundary network

Reports by other authors demonstrate that the proton conductivity of grain boundaries increases as grain size decreases [15]. This effect is particularly noticeable in nanomaterials with a grain size of less than 20 nm, which exhibit significant proton conduction even at room temperature when exposed to humidity [25]. TEM analysis (Figure 2) shows that the nanoparticles tend to form agglomerations. These create a dense network of grain boundaries, crucial for the formation of interconnected proton conduction pathways [16]. Therefore, our use of nanoparticles in the 7–10 nm range provides an extremely high surface-to-volume ratio, which significantly enhances the number of active sites available for water adsorption, amplifying the effect of the first mechanism. As a result, the internal pore network becomes progressively saturated, and more hydroxyl groups form over time, leading to a gradual increase in proton conductivity. [20,15]

4.2. Model Representation of the Experimental Equivalent Circuit

Assuming that the overall frequency response of the electrochemical cell can be modeled in terms of a simple equivalent circuit, the YSZ sensors could also be modeled using equivalent circuits.

Figure 6 shows six simple equivalent circuits and their representations in the Z(f) geometric plane. The values R, C and Q are resistance, capacitance and constant phase element, respectively. The equivalent circuit corresponding to our sensors, shown in Figure 7, is obtained by combining the circuits shown in Figure 6.

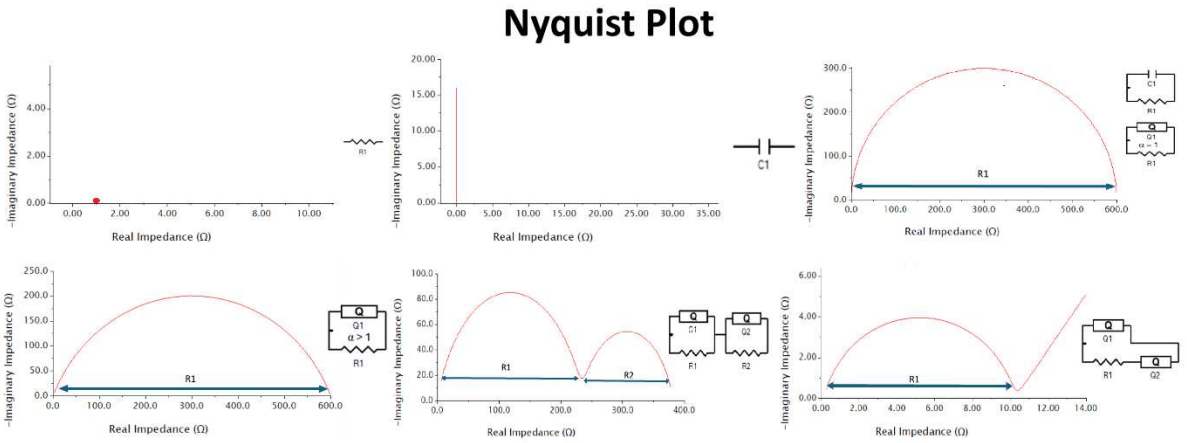


Figure 6. Complex impedance graphics for R-Q-Z(f) circuits.

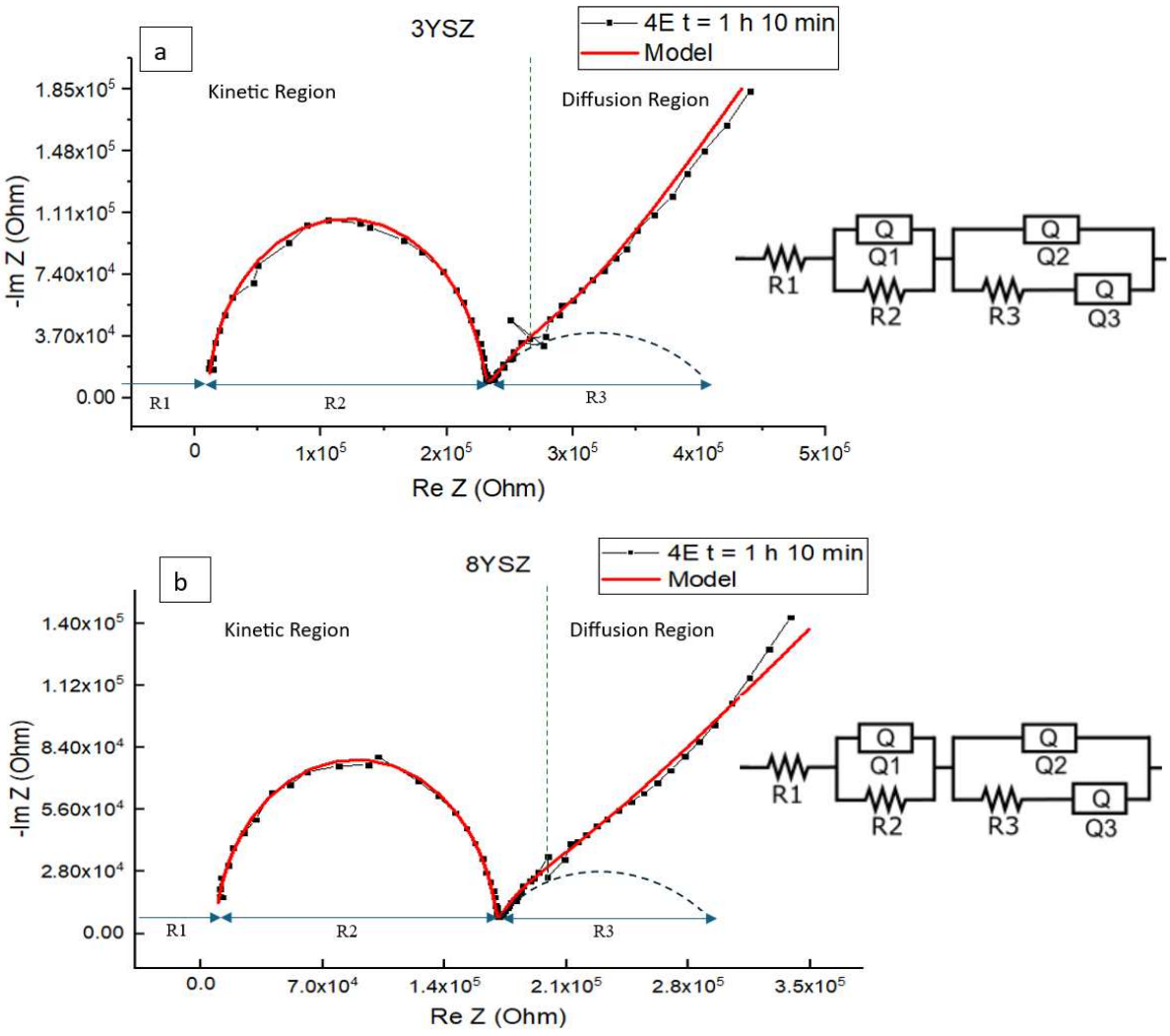


Figure 7. Complex impedance graphics for 3YSZ (a) and 8YSZ (b) sensors.

Figure 7 presents the impedance graph of 3YSZ (a) and 8YSZ (b) samples, with their respective equivalent circuits, distinguishing two regions of interest: the kinetic region at high frequencies and the diffusion region at low frequencies [26].

It can be observed that two semicircles appear in the kinetic region, which are associated with the electrical resistivity of the material. R_1 (high frequency) corresponds to the characteristic bulk resistance (intrinsic ionic conduction within the nanoparticles), while R_2 (intermediate frequency) is attributed to the grain boundary resistance (surface-related conduction). R_3 corresponds to the resistance associated with the diffusion of reactive species through the hydrated surface layer. The constant phase element Q_3 is used to express the impedance related to the diffusion of reactive species, taking into account non-ideal behavior due to surface roughness, porosity, or a distribution of diffusion path lengths [19].

4.3. Integrated model of the transport model and equivalent circuit model

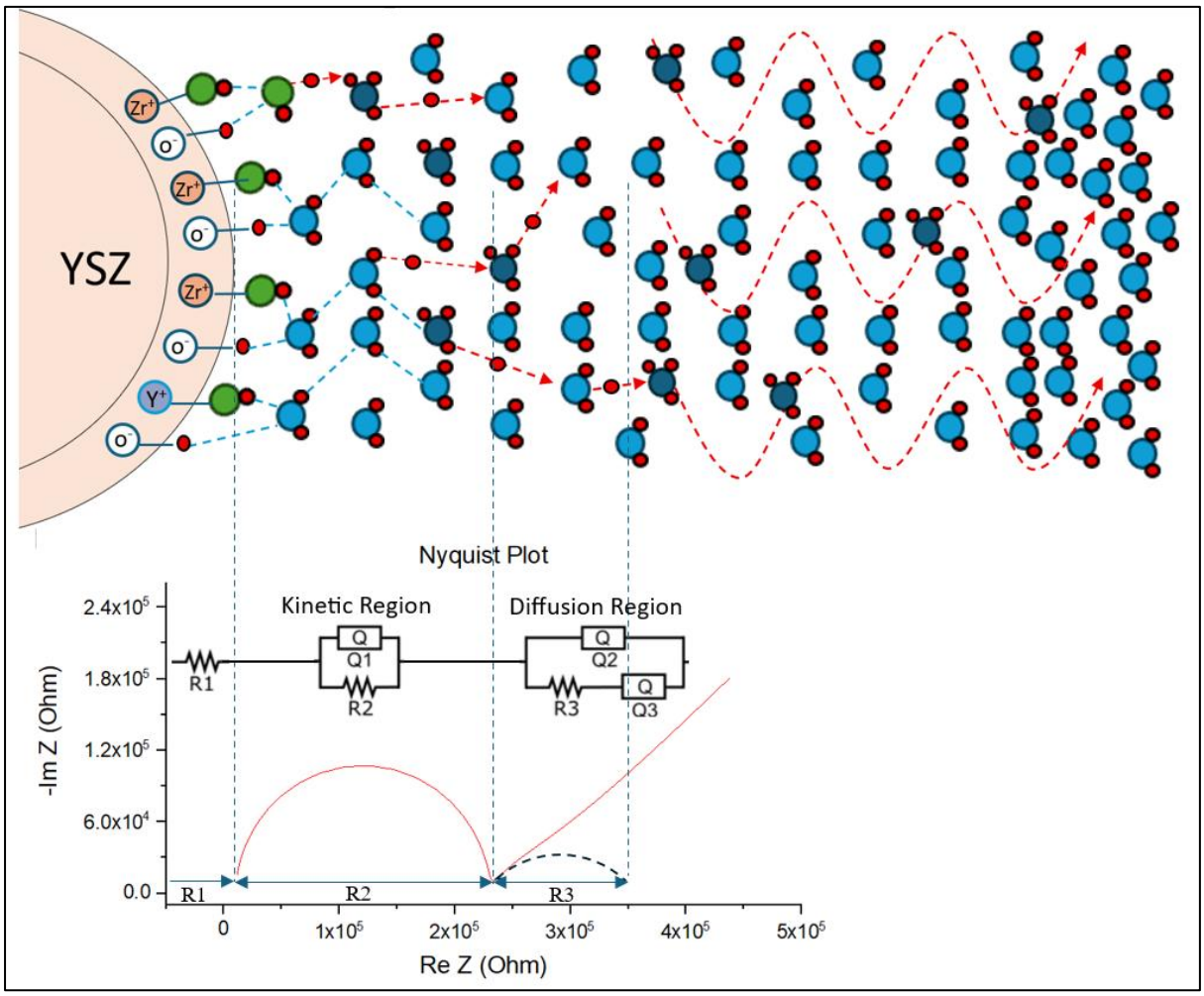


Figure 8. Schematic interpretation of the hydration process of YSZ sensors incorporating the charge carrier transport model and the equivalent circuit model.

Figure 8 graphically shows the complementarity of the two models analyzed previously (charge carrier transport model and equivalent circuit model), providing a coherent framework to explain and quantify the experimental behavior observed in the 3YSZ and 8YSZ sensors, under high relative humidity conditions of 100%. It establishes correspondences between the physicochemical phenomena that occur on the surface of the nanoparticle and the electrical elements of the equivalent circuit, which allows a systematic interpretation of the characteristic impedance changes presented in Figure 7, and Tables 1 and 2.

YSZ 3%	Exp.	R_1 (Ω)	R_2 (Ω)	R_3 (Ω)	Q_1 (s^q/Ω)	α_1	Q_2 (s^q/Ω)	α_2	Q_3 (s^q/Ω)	α_3	X^2 (chi-squared)
Sample											
1S	2E	9528	516538	284803	1.31E-11	0.9806	3.17E-07	0.6223	8.91E-07	0.5379	0.0265
	3E	9202	317267	193671	1.29E-11	0.9820	4.33E-07	0.6047	1.07E-06	0.5120	0.0441
	4E	9728	218071	157009	1.28E-11	0.9870	4.64E-07	0.6179	1.21E-06	0.5120	0.0546
3S	2E	9508	437239	102269	1.54E-11	0.9668	1.94E-07	0.6776	1.50E-06	0.5480	0.0552
	3E	9112	289167	73337	1.57E-11	0.9684	1.31E-07	0.7503	1.73E-06	0.5845	0.0217
	4E	8937	194870	53235	1.39E-11	0.9818	2.45E-07	0.6707	2.18E-06	0.5649	0.0306
5S	2E	9404	279971	406903	1.34E-11	0.9821	3.53E-07	0.4776	3.79E-07	0.4493	0.0567
	3E	9552	189915	341150	1.49E-11	0.9757	3.93E-07	0.4961	4.46E-07	0.4461	0.0311
	4E	9655	126211	241318	1.58E-11	0.9779	4.92E-07	0.4931	6.17E-07	0.4595	0.0570

Table 1: Experimental values of resistance and CPE parameters for 3YSZ sensors

YSZ 8%	Exp.	R_1 (Ω)	R_2 (Ω)	R_3 (Ω)	Q_1 (s^q/Ω)	α_1	Q_2 (s^q/Ω)	α_2	Q_3 (s^q/Ω)	α_3	X^2 (chi-squared)
Sample											
2S	2E	8989	532553	359905	1.30E-11	0.9849	3.38E-07	0.5995	9.70E-07	0.6062	0.0181
	3E	9198	237146	156877	1.32E-11	0.9869	2.70E-07	0.6868	1.48E-06	0.5395	0.0246
	4E	7850	160412	97883	1.42E-11	0.9850	2.67E-07	0.7120	1.89E-06	0.5198	0.0237
4S	2E	8012	323599	892517	1.56E-11	0.9737	8.18E-07	0.4302	1.89E-07	0.1858	0.0438
	3E	7468	220058	350164	1.79E-11	0.9633	7.53E-07	0.4797	3.33E-07	0.2696	0.0612
	4E	7792	149109	259961	1.69E-11	0.9757	9.38E-07	0.4802	5.48E-07	0.2634	0.0537
6S	2E	7939	520794	7715060	1.58E-11	0.9708	7.83E-08	0.5728	2.48E-07	0.2888	0.0638
	3E	8628	350442	1231160	1.50E-11	0.9745	8.49E-08	0.5989	1.33E-07	0.1172	0.0538
	4E	7409	219841	706199	1.83E-11	0.9640	9.03E-08	0.6198	2.04E-07	0.2340	0.0614

Table 2: Experimental values of resistance and CPE parameters for 8YSZ sensors

It can be observed that for both 3YSZ and 8YSZ, the R_1 resistance value remains almost unchanged, primarily due to the low penetration of water into the bulk. It should be noted that R_1 for 8YSZ is lower compared to 3YSZ, consistent with its higher ionic conductivity due to a greater number of oxygen vacancies.

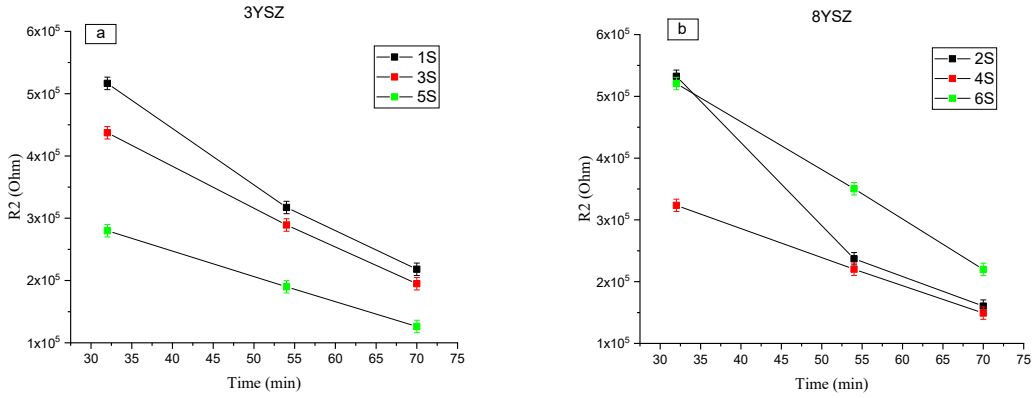


Figure 9. Decrease of R_2 as a function of time for 3YSZ (a) and 8YSZ (b).

Regarding the systematic decrease in R_2 with exposure time, this is directly related to the formation of the proton conduction pathway on the hydrated surface and the progressive saturation of the hydroxyl network. As mentioned previously, this is due to the formation of physisorption layers and the activation of the Grotthuss mechanism, which reduces the resistance to proton flow between particles. As shown in Figure 9, both 3YSZ and 8YSZ demonstrate the ability to adsorb water and conduct protons at grain boundaries. Tables 1 and 2 show that no qualitative differences attributable to yttrium concentration are observed, as the reduction of R_2 is approximately 50–70% in all cases.

In contrast, R_3 decreases systematically with exposure time, indicating that the diffusion network continues to evolve and improve with hydration.

Discussion

This study investigated the effect of humidity on the electrical impedance of zirconia nanoparticles stabilized with two different yttria contents (3 mol% and 8 mol% Y_2O_3) under 100% relative humidity at four different exposure times (4, 32, 54, and 70 minutes).

(i) The ionic conduction process was described using the charge-carrier transport model. The impedance study is consistent with humidity-induced proton conduction being the dominant mechanism. Based on literature concerning similar systems, conduction is expected to proceed via Grotthuss and vehicular mechanisms [22, 23, 27]. The increase in water adsorption and proton mobility is attributed to the high density of surface-active sites resulting from the small particle size (7–10 nm).

(ii) To monitor the evolution of the impedance response, an equivalent circuit was developed that combines bulk (high frequency), grain boundary (intermediate frequency) contributions, along with a diffusion element (low frequency), to model the impedance response of the 3YSZ and 8YSZ sensors under high humidity conditions.

(iii) Under these conditions, three main processes can be distinguished: R_1 (high frequency) represents bulk ion conduction within the nanoparticles, which is practically unaffected by humidity. R_2 (intermediate frequency) corresponds to the grain boundary resistance, which is highly sensitive to water adsorption and proton transport at the grain boundaries. R_3 (low frequency) represents the resistance associated with the diffusion of reactive species through the hydrated surface layer.

(iv) No qualitative differences were observed in the humidity-induced proton conduction process at the grain boundaries between 3YSZ and 8YSZ, since both compositions exhibit a clear time-dependent decrease in R_2. It is important to note, however, that although the percentage decrease in R_2 is comparable for both materials (approximately 50-70% in all cases), the absolute value of R_1 (volumetric resistance) is lower for 8YSZ than for 3YSZ (Tables 1 and 2). This is consistent with the higher concentration of oxygen vacancies in 8YSZ, which increases the ionic conductivity of the material. This confirms that the ability to adsorb water and conduct protons via the Grotthuss and vehicular mechanisms is not determined by the yttria content. These findings suggest that surface-related phenomena dominate over bulk vacancy concentration in the nanoscale regime under high humidity.

(v) The findings gained from this study on the humidity-induced proton conduction mechanism in YSZ nanopowders establish a foundation for their application as humidity-activated gas sensors operating at room temperature.

Funding

This work was supported by the Serbia—JINR cooperation Projects №.109 2026 items 9, Serbia—JINR cooperation Projects №676 2025 items №7, 21 and 26, Belarus—JINR cooperation Projects №. 302 / 2026 item 18, Kazakhstan – JINR № 111 2026, item 13. JINR – Arab Republic of Egypt №127 / 2026г, item 8.

Conflict of Interest

The authors declare that they have no known competing financial interests or personal relationships that could have appeared to influence the work reported in this paper.

References

[1] Vendrell X, West AR (2018) Electrical properties of yttria-stabilized zirconia, YSZ single crystal: local AC and long range DC conduction. J Electrochem Soc 165:F966–F975. https://doi.org/10.1149/2.0881811jes

[2] Asgerov EB, Beskrovnyy AI, Doroshkevich NV, Mita C, Mardare DM, Chicea D, et al (2022) Reversible martensitic phase transition in yttrium-stabilized ZrO2 nanopowders by adsorption of water. Nanomaterials 12:435. https://doi.org/10.3390/nano12030435

[3] Badwal SPS (1992) Zirconia-based solid electrolytes: microstructure, stability and ionic conductivity. Solid State Ionics 52:23–32. https://doi.org/10.1016/0167-2738(92)90088-7

[4] Shylo A, Doroshkevich A, Lyubchyk A, Bacherikov Y, Balasoiu M, Konstantinova T (2020) Electrophysical properties of hydrated porous dispersed system based on zirconia nanopowders. Appl Nanosci 10:4395–4402. https://doi.org/10.1007/s13204-020-01471-2

[5] Thiel PA, Madey TE (1987) The interaction of water with solid surfaces: fundamental aspects. Surf Sci Rep 7:211–385. https://doi.org/10.1016/0167-5729(87)90001-X

[6] Köck EM, Kogler M, Klötzer B, Noisternig MF, Penner S (2016) Structural and electrochemical properties of physisorbed and chemisorbed water layers on the ceramic oxides Y2O3, YSZ, and ZrO2. ACS Appl Mater Interfaces 8:16428–16443. https://doi.org/10.1021/acsami.6b03566

[7] Doroshkevich AS, Lyubchyk AI, Shilo AV, Zelenyak TY, Glazunova VA, Burhovetskiy VV, et al (2017) Chemical-electric energy conversion effect in zirconia nanopowder systems. J Surf Investig 11:523–529. https://doi.org/10.1134/S1027451017030053

[8] Bauerle JE (1969) Study of solid electrolyte polarization by a complex admittance method. J Phys Chem Solids 30:2657–2670. https://doi.org/10.1016/0022-3697(69)90039-0

[9] Irvine JTS, Sinclair DC, West AR (1990) Electroceramics: characterization by impedance spectroscopy. Adv Mater 2:132–138. https://doi.org/10.1002/adma.19900020304

[10] Yaman YT (2020) Development of electrochemical impedimetric sensors and applications. PhD thesis, Hacettepe University, Ankara

[11] Štukovnik Z, Fuchs-Godec R, Bren U (2023) Nanomaterials and their recent applications in impedimetric biosensing. Biosensors 13:899. https://doi.org/10.3390/bios13100899

[12] Hernandez MA, West AR (2015) Dipolar relaxation and impedance of an yttria stabilised zirconia ceramic electrolyte. J Mater Chem A 3:1298–1305. https://doi.org/10.1039/c5ta08990e

[13] Matsui N (1992) Equivalent circuit analysis of mixed conductor/electrode system by impedance spectroscopy. Solid State Ionics 57:121–124. https://doi.org/10.1016/0167-2738(92)90073-X

[14] Aftermath Software (2022) Release 1.6.10523. Pine Research Instrumentation, Durham

[15] Avila-Paredes HJ, Zhao J, Kim S, et al (2010) Protonic conductivity of nano-structured yttria-stabilized zirconia: dependence on grain size. J Mater Chem 20:990–994. https://doi.org/10.1039/b919100c

[16] Miyoshi S, Akao Y, Kuwata N, Kawamura J, Oyama Y, Yagi T, Yamaguchi S (2012) Water uptake and conduction property of nano-grained yttria-doped zirconia fabricated by ultra-high pressure compaction at room temperature. Solid State Ionics 207:21–28. https://doi.org/10.1016/j.ssi.2011.11.014

[17] Park H, Cho E, Zou Y, Lee S, Choi J, Lee SB, et al (2023) Synthesis of yttria-stabilized zirconia nanospheres from zirconium-based metal–organic frameworks and the dielectric properties. Nanomaterials 13:28. https://doi.org/10.3390/nano13010028

[18] Huang D, Venkatachari KR, Stangle GC (1995) Influence of yttria content on the preparation of nanocrystalline yttria-doped zirconia. J Mater Res 10:762–773. https://doi.org/10.1557/JMR.1995.0762

[19] Barsoukov E, Macdonald JR (eds) (2005) Impedance spectroscopy, 2nd edn. John Wiley & Sons, Inc.

[20] Morimoto T, Nagao M, Tokuda F (1969) The relation between the amounts of chemisorbed and physisorbed water on metal oxides. J Phys Chem 73:243–248. https://doi.org/10.1021/J100721A039

[21] Raz S, Sasaki K, Maier J, Riess I (2001) Characterization of adsorbed water layers on Y2O3-doped ZrO2. Solid State Ionics 143:181–204. https://doi.org/10.1016/S0167-2738(01)00826-8

[22] Kreuer KD (1996) Proton conductivity: materials and applications. Chem Mater 8:610–641. https://doi.org/10.1021/cm950192a

[23] Stub SØ, Vollestad E, Norby T (2017) Mechanisms of protonic surface transport in porous oxides: example of YSZ. J Phys Chem C 121:12817–12825. https://doi.org/10.1021/acs.jpcc.7b03005

[24] Jiang JJ, Hertz JL (2014) Intermediate temperature surface proton conduction on dense YSZ thin films. J Mater Chem A 2:19550–19555. https://doi.org/10.1039/C4TA01858C

[25] Chiodelli G, Maglia G, Anselmi-Tamburini S, Munir ZA (2009) Characterization of low temperature protonic conductivity in bulk nanocrystalline fully stabilized zirconia. Solid State Ionics 180:297–301. https://doi.org/10.1016/j.ssi.2009.02.031

[26] Doroshkevich AS, Lyubchyk AI, Oksengendler BL, Zelenyak TY, Appazov NO, Kirillov AK, et al (2022) Electric energy storage effect in hydrated ZrO2-nanostructured system. Nanomaterials 12:1783. https://doi.org/10.3390/nano12111783

[27] Celik E, Negi RS, Bastianello M, Boll D, Mazilkin A, Brezesinski T, Elm MT (2020) Tailoring the protonic conductivity of porous yttria-stabilized zirconia thin films by surface modification. Phys Chem Chem Phys 22:11519–11528. https://doi.org/10.1039/D0CP01619E